

Further investigation of spatially resolved single grain quartz OSL and TL signals

Julie A. Durcan^{a,*}, Geoff A.T. Duller^b

^a School of Geography and the Environment, University of Oxford, Oxford, OX1 3QY, UK

^b Department of Geography and Earth Sciences, Aberystwyth University, Aberystwyth, SY23 3DB, UK

ARTICLE INFO

Keywords:

Components
Characteristic dose
EMCCD
OSL
Quartz
Single grain
TL

ABSTRACT

The use of luminescence signals from single mineral grains for optical dating has become a valuable and frequently utilised tool in Quaternary Geochronology. Single grain luminescence dating is particularly beneficial in complex depositional settings, however the ability to measure single grain signals also offers the opportunity to assess intrinsic luminescence properties of individual mineral grains. The use of spatially resolved luminescence technologies such as an electron multiplier charge coupled device is of benefit when making luminescence measurements at single grain scales because they allow stimulation with light emitting diodes, and this offers a number of key benefits related to stimulation power when it comes to the assessment of characteristics such as optically stimulated luminescence (OSL) decay rate and the calculation of parameters such as the fast ratio and photo ionisation cross-sections. In this paper, the intra- and inter-sample variability of sensitised single grain thermoluminescence (TL) and OSL signals is considered. A comparison between TL and OSL signals is undertaken, as well as calculation of the fast ratio, OSL component photo ionisation cross-sections, thermal stability, and characteristic dose for a suite of quartz samples from a range of geographic locations and depositional settings. For these heated signals, key findings include the lack of relationship between OSL signal intensity and dominance of the fast component, the fitting of two components (a fast and slow component) is the most common fit for single grain OSL signals, characteristic doses from fast dominated signals suggesting saturation at c. 150 Gy, and the identification of the ultrafast OSL component. Intra-sample variability across all measured parameters is observed, suggesting that for this suite of samples, variability is the norm rather than the exception, and that the intrinsic luminescence characteristics of quartz are variable and diverse.

1. Introduction

The use of luminescence signals from single mineral grains for optical dating purposes has become a valuable and widely applied tool in Quaternary Geochronology. It has particular benefit for the dating of complex sedimentary environments, and for example, in contexts where a skewed or broadly distributed equivalent dose (D_e) distribution may arise from issues such as incomplete bleaching (e.g. Rodnight et al., 2006) and/or post-depositional mixing (e.g. Kristensen et al., 2015). In these types of settings, the use of optical signals from single grains can yield the 'true' burial D_e in the absence of signal averaging which may be a feature of multi-grain luminescence signals. Single grain luminescence analysis not only benefits dating applications, but offers the opportunity to assess intrinsic luminescence properties of individual mineral grains (e.g. Duller, 2008). Intra- and inter-sample variability in the

characteristics and kinetic properties of quartz luminescence signals has long been observed, including variability in thermoluminescence (TL) signal shapes (Adamiec, 2000; Durcan and Duller, 2022), optically stimulated luminescence (OSL) yield and sensitivity (Duller et al., 2003; Durcan and Duller, 2022), OSL decay rate (Adamiec 2005; Durcan and Duller 2022), thermal stability (Rui et al., 2019), and the presence and composition of different quartz OSL components (Bulur et al., 2002; Durcan and Duller, 2022). A more comprehensive understanding of the intrinsic variability of quartz OSL signals not only benefits dating outcomes, for example through the identification of signals with properties most desirable for dating (e.g. Smedley et al., 2019; Hu et al., 2021), but also may benefit emerging techniques which make use of luminescence signals beyond dating applications, such as sediment provenance and pathway tracers techniques (e.g. Gray et al., 2019).

The development of the automated focussed laser attachment for the

* Corresponding author.

E-mail address: julie.durcan@ouce.ox.ac.uk (J.A. Durcan).

<https://doi.org/10.1016/j.radmeas.2024.107260>

Received 15 November 2023; Received in revised form 3 July 2024; Accepted 25 July 2024

Available online 26 July 2024

1350-4487/© 2024 The Authors. Published by Elsevier Ltd. This is an open access article under the CC BY license (<http://creativecommons.org/licenses/by/4.0/>).

Risø TL/OSL luminescence readers in the early 2000s (e.g. Duller et al., 1999; Bøtter-Jensen et al., 2000, 2003) has facilitated the routine and rapid measurement of single grain signals, and allows 100s–1000s of grains to be readily measured. Using the focussed laser system, individual mineral grains are stimulated with a 20 μm diameter laser beam, and the resulting luminescence is detected using a photomultiplier tube (PMT). However, the use of the focussed laser system for single grain measurements results in some additional uncertainties when compared to signal measurement using light emitting diodes (LEDs). Thomsen et al. (2012, 2015) report that optical stimulation using the laser cannot be considered constant through a single grain measurement run using the system, because using a narrow laser beam for stimulation relies upon light scattering within the grain hole to fully illuminate the grain (Thomsen et al., 2012). Durcan and Duller (2022) comment that other unknowns such as grain variability (e.g. opacity, colour, surface condition, position within the measurement hole) and instrumental uncertainties such as the laser angle of incidence and effective stimulation power at the grain location may also affect stimulation power. As such, an absolute value for the effective stimulation power from the laser cannot be quantified, although power density is typically much higher ($\sim 10 \text{ W/cm}^2$) than from the LEDs ($\sim 10\text{--}100 \text{ mW/cm}^2$) used for multi-grain measurements. The inability to quantify stimulation power is undesirable because it prevents the determination of kinetic parameters, such as the photo ionisation cross-section, from single grain signals, and a lack of consistent stimulation power through a measurement run may have unquantifiable effects on the accuracy of D_e determinations.

The recently developed spatially resolved Risø attachment (Kook et al., 2015) makes use of an electron multiplying charge-coupled device (EMCCD) camera to make luminescence measurements, and offers an alternative means of measuring single grain luminescence signals. Using this system, all grains are stimulated simultaneously with LEDs, and the resulting luminescence signals are imaged rather than detected using a PMT. Whilst detection sensitivity is lower than the focussed laser system (e.g. Thomsen et al., 2015), use of the EMCCD system offers a number of benefits and circumvents some of the uncertainties associated with ascertaining the effective stimulation power provided by the laser. As mentioned, the lower power density of the LEDs can benefit mathematical treatment of luminescence signals, such as curve deconvolution where the mathematical fitting of multiple exponential functions can be a challenge (Istratov & Vyvenko, 1998; Bailey, 2010), which can be improved in instances where component decay rate increases (Bailey, 2010). The imaging of luminescence allows single grain thermoluminescence (TL) as well as optically stimulated luminescence (OSL) signals to be assessed. This has the benefit of being able to view behaviours of the luminescence traps via the TL signals, as well as the radiative luminescence centres responsible for producing OSL.

This study aims to investigate intra- and inter-sample variability of quartz luminescence signals using the EMCCD system to provide spatially resolved luminescence measurements, and further develops the study of Durcan and Duller (2022). Two key parameters of the quartz OSL signal are investigated. The first is the presence and dominance of the fast OSL component, using the fast ratio and mathematical determination of the photo ionisation cross-sections from the single grain signals, expanding the analysis from the brightest 50 grains of the dataset (Durcan and Duller, 2022) to all single grain signals with a detectable signal ($n = 214$). The second is the characteristic dose (D_0), frequently considered as a determinant of signal saturation levels, and mathematically calculated from dose response curves with an upper regenerative dose of 1000 Gy. Signal sensitivity will be considered, and the link between OSL signal characteristics and TL decay curve form will be investigated.

2. Methods

Single grain OSL and TL measurements were made at the

Aberystwyth Luminescence Research Laboratory, Aberystwyth University using a Risø TL/OSL DA-20 luminescence reader. Spatially resolved luminescence signals were detected using a high sensitivity Photometrics Evolve 512 EMCCD camera attachment (Kook et al., 2015), and ultraviolet quartz signals were detected through a combination of 3 mm Hoya U340 and 2 mm UG-11 filters. Signal stimulation was undertaken using blue light emitting diodes (LEDs) with a wavelength of 470 nm and an estimated stimulation power of 30 mW/cm^2 at the grain location (Durcan and Duller, 2022), and stimulation using infrared (IR) LEDs (870 nm) was used to check for contamination of the quartz signal by IR-responsive minerals. Radiation doses were administered using a calibrated $^{90}\text{Sr}/^{90}\text{Y}$ beta source with a dose rate of 6.1 Gy/min. Image processing used a Matlab image-processing algorithm in Viewer + to identify the positions of each single grain disc during measurement (Kook et al., 2018). TL and OSL signals were then spatially integrated from circular region of interest (ROI) with a diameter of 300 μm centred on each grain hole.

Single grains of quartz were loaded into aluminium sample discs, containing 100 grain holes (in a 10 by 10 array) of 300 μm diameter and depth. Discs were visually inspected prior to measurement to ensure that all holes were filled with a single grain and to remove excess grains from the surface of the sample disc. Prior to measurement, grains were annealed using ten cycles of radiation dosing and TL up to 450 °C. For the experiments presented in this study, TL measurements up to 450 °C (heating rate 5 °C/s and channel width 1 °C) were made following a 75 Gy dose and a pause of 3600 s to allow for a reduction of the signal intensity of the 110 °C TL peak in order to better view the remaining TL signal. Where TL signals from individual peaks are considered, signal from ± 15 °C around the peak was summed, and the total TL signal is considered as the signal arising from 50 °C–450 °C heating, with the averaged signal from 0 to 20 °C subtracted as the background. OSL measurements were made following a single aliquot regenerative dose (SAR) protocol (e.g. Murray and Wintle, 2000), and measurement of the OSL signals (at 125 °C for 100 s, with a channel width of 0.15 s) were made following a pre-heat of 220 °C for 10 s and a cut-heat of 160 °C for 10 s. Grains were defined as giving light if the test dose signal was $> 3\sigma$ above background (Jacobs et al., 2006), signals where the maximum test dose uncertainty was $< 20\%$ (Peng and Li, 2017; Hu et al., 2021), and the reduced chi-squared for the dose response curve fit was < 5 (Peng and Li, 2017; Hu et al., 2021) were included in analysis. Signal intensity and fast ratios values were calculated using OSL signals following a 75 Gy dose. OSL curves were integrated using a late background subtraction, where signals from the first 1.5 s of stimulation were used, and a background averaged from the final 15 s was subtracted. The fast ratio $[(L1-L3)/(L2-L3)]$; Durcan and Duller, 2011) was calculated using signal from the first 0.15 s of stimulation (L1), 1.95–2.10 s (L2), and the averaged signal between 14.1 and 20.55 s (L3). Curve deconvolution was undertaken using OSL signals measured following a 75 Gy dose and the R Luminescence package (Kreutzer et al., 2023) was used for fitting. D_0 values were calculated from dose response curves constructed using regenerative doses of up to 1000 Gy that were fitted with a single saturating exponential function. A pulse annealing test was also undertaken on the same grains using the SAR protocol described, using a 75 Gy dose, and heating to temperatures between 200 °C and 400 °C at 20 °C intervals instead of using the fixed pre-heat temperature (Table S1), and a hot bleach at 280 °C for 100 s was included at the end of each SAR cycle (e.g. Fan et al., 2011).

This study furthers the results and analysis presented by Durcan and Duller (2022). It uses the same 8 quartz samples, selected to represent a range of depositional environments, geographical locations, and quartz signal properties at multi-grain scales of analyses, and are summarised in Table 1. Single grain OSL and TL signals from the 10 signals with the highest OSL signal intensity are shown in Fig. S1, alongside multi-grain OSL and TL curves for all samples (Fig. S2), which were derived from the sum of single grain signals.

Table 1

The samples used in this study. 100 sediment grains were measured for each sample, and the number of OSL signals indicates the number of signals satisfying the rejection criteria ($n = 214$). The mean OSL signal intensity (from channel 1, 0–0.15 s) is shown, as well as the OSL signal intensity at the first (Q25), second or median (Q50), and the third (Q75) quartile.

Location	Sample name	Depositional context	Grain size (μm)	Number of OSL signals	Average OSL signal intensity (\pm standard deviation)	OSL signal intensity at Q25, Q50, Q75
Calibration Quartz (Batch 113)	CalQtz	Annealed sediment	180–250	69	1036 \pm 2625	154, 260, 820
Malawi	MAL05/01/01	Lake shoreline sand	180–212	39	466 \pm 1088	144, 243, 335
Zambia	105/KB1	Palaeochannel sand	180–212	41	867 \pm 2625	139, 212, 551
Tasmania	TNE9726	Aeolian dune sand	180–250	39	1140 \pm 4772	101, 142, 416
UK	78/NO4	Glaciofluvial outwash	180–212	0	0	
USA	84/LSM6	Beach barrier overwash sand	180–212	10	2107 \pm 5055	57, 85, 1427
Cyprus(1)	108/AGN2	Coastal, beach sand	180–212	7	1512 \pm 3574	104, 145, 269
Cyprus(2)	109/MAZ2	Coastal, beach sand	180–212	9	428 \pm 400	97, 363, 763

3. Results and discussion

3.1. Luminescence signal intensity

OSL signal intensity and yield are often reported in luminescence dating studies, however because the focussed laser system does not offer the possibility of making single grain TL measurements, the relationship between TL and OSL at single grain scales is relatively unknown. Use of the EMCCD systems offers this option, and in Fig. 1a, background-subtracted total TL counts and total OSL counts are compared for all signals ($n = 800$) measured in this study. Signals integrated from the 110 °C, 170 °C, 230 °C, 325 °C, and 375 °C TL peaks compared with the OSL are also shown (Fig. 1b). For individual single grain signals, signal counts from both OSL and TL varies across a range of 10^1 – 10^5 counts (10^0 – 10^4 at single grain scale), although there is a tendency towards higher signal intensities in OSL signals in comparison to TL. Whilst the number of grains that yield OSL varies between samples (Table 1), there is no sample dependence on intensity, with individual grains from the same samples yielding luminescence intensities which vary across the full range of intensities (see also Durcan and Duller, 2022). There is no strong statistical relationship between total OSL and TL signal intensity ($R^2 = 0.65$), nor OSL and individual TL peak signal intensity, with coefficient of determination values of 0.60 for the 110 °C TL peak and similar values indicative of a weak correlation for the 170 °C ($R^2 = 0.50$), 230 °C ($R^2 = 0.56$), 325 °C ($R^2 = 0.47$), and 375 °C ($R^2 = 0.37$) peaks. There is no clear, strong positive correlation between OSL signal intensity (in the initial part of the signal) and any of the TL peaks. Whilst Spooner (1994) suggests the 325 °C TL peak is responsible for the production of OSL signals, there is not a clear indication of this in this

dataset when considering the composite luminescence signal in the initial part of the OSL decay curve. This favours the findings of Kitis et al. (2010), who suggest that there is no specific relationship between the fast component and specific TL peaks. The presence and magnitude of different quartz OSL components as a variable is considered in section 3.2 to check whether the presence/absence of different quartz OSL components may impact this relationship.

An additional feature of the dataset is the asymmetry often seen in the TL and OSL sensitivity from an individual grain following dosing (Fig. 1a), whereby some grains produce a detectable ultra-violet (UV) TL signal but not a UV OSL signal or vice versa. For example, there are a subset of grains producing reasonably bright (>1000 counts in channel 1) OSL signals, yet have a limited TL response (<100 counts), and vice versa with bright TL signals (almost 10,000 counts) produced from grains which show a limited OSL response. Sedimentary quartz has been shown to have a number of TL emissions (e.g. Hashimoto et al., 1986; Rink et al., 1993) and as summarised by Krbetschek et al. (1997), quartz has prominent emissions in the UV wavelength range (360–420 nm), the blue (460–480 nm) and the orange-red (610–630 nm). It is therefore possible that for those grains with a detectable UV OSL signal but no/low TL may be emitting TL non-UV wavelengths, which are undetectable with the filter pack combination selected (section 2). An explanation for why some grains provide TL but no UV OSL signal is more difficult to come by. The emission spectra of quartz OSL is less well investigated (Lomax et al., 2015), although appears to be for the most part limited to a broad UV emission. For sedimentary quartz, Huntley et al. (1991) report a quartz UV emission at ~ 365 nm and a much weaker emission in the UV-blue (400–500 nm), and using synthetic quartz, Martini et al. (2009) report similar findings, with a broad quartz emission between

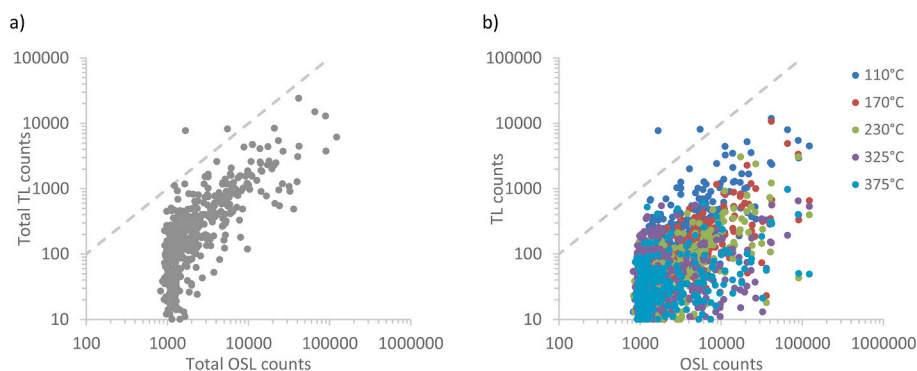


Fig. 1. OSL and TL signal intensities. In a) total OSL (signal summed from across the whole stimulation period with an background subtracted from the period when counts were recorded without stimulation) and total TL (signal summed from across the 50–450 °C, with the average counts from 0 to 49 °C subtracted) are plotted, and in b) total OSL is plotted against the signal intensities from TL peaks 110 °C, 170 °C, 230 °C, 325 °C, and 375 °C, with signals integrated from ± 15 °C range around the peak. Note, after dosing, a 1000 s pause was incorporated prior to measurement of the TL signal to allow for a reduction in the magnitude of the 110 °C TL peak intensity. The 1:1 line is shown by the dashed line.

250 and 410 nm, centred at ~ 380 nm. This suggests that OSL should be emitted in the UV range. One hypothesis to explain grains that emit UV TL but not OSL may be a limitation of and/or change to the availability of luminescence centres, pathways between TL traps and optical centres, or optical de-sensitisation processes (c.f. McKeever and Morris, 1994; Bailey, 2001). A simple comparison between TL and OSL signal intensities is not sufficient to be able to explain the lack of correlation between the two for this dataset, but it does offer an intriguing hint of the complexity of relationship between trap, recombination centres, and the pathways between the two at single grain scales of analysis.

3.2. Quartz OSL components

The quartz OSL signal is comprised of a number of individual components, termed the fast, medium and slow (e.g. Bailey et al., 1997; Jain et al., 2003; Singarayer and Bailey, 2003). OSL signals from these individual components are sourced from different traps within quartz crystals, and have variable properties such as stability and bleaching, as well as different trap kinetic parameters which results in differing rates of charge detrapping (e.g. Bailey et al., 1997). For dating purposes, OSL signals which are dominated by the fast component in the initial part of the OSL signal are desirable, because the fast component is stable over the dateable range of luminescence dating, it is bleached rapidly upon exposure to daylight, and the SAR protocol was tested on fast component-dominated samples (e.g. Wintle and Murray, 2006). Contributions from non-fast OSL components can provide erroneous results when dating, and non-fast component-dominated signals are usually considered undesirable for dating applications (e.g. Choi et al., 2003; Jain et al., 2005; Durcan and Duller, 2011).

A lack of correlation between the fast ratio and OSL signal intensity

for the brightest 50 grains in this dataset has already been reported by Durcan and Duller (2022), and extending this analysis to all signals passing the signal intensity rejection criteria ($n = 214$), Fig. 2a shows that this relationship remains the case. This contrasts to other studies such as Hu et al. (2021) where a more positive correlation has been observed. Of the assessed 214 signals, 108 signals yield fast ratios greater than 20, indicative of dominance of the fast component in the initial part of the signal (Durcan and Duller, 2011). The calibration quartz sample has the highest proportion of fast dominated signals, with 44 of the 69 grains having a fast ratio > 20 . The other samples have a lower proportion of fast component-dominated signals e.g. Malawi 14/39, Zambia 18/41, and Tasmania 22/39 grains. Interestingly, even samples specifically selected for use due to their lack of a fast component at a multi-grain scale include signals which pass the fast ratio: 1/7 signals for Cyprus1 sample, and 1/10 signals for Cyprus2. This suggests that a lack of dominance of the fast component at multi-grain scales does not necessarily indicate a lack of fast component-dominated OSL signals at single grain scales. When summing the signal from all grains on each disc to reproduce a multi-grain signal, the effects of signal averaging can be clearly seen, with fast ratios of CalQtz 78.6 ± 3.1 , Malawi 25.2 ± 1.2 , Zambia 39.0 ± 1.9 , Tasmania 62.43 ± 2.54 , USA 62.1 ± 3.6 , Cyprus (1) 9.1 ± 0.3 , Cyprus (2) 4.8 ± 0.2 . For samples lacking fast component-dominated signals at multigrain scales, and where the use of other dosimeters such as feldspar is not an option, moving to single grain measurements may offer fast component-dominated signals for dating.

Mathematical deconvolution of the single grain OSL signals was undertaken to identify presence and composition of the quartz OSL components. Signals were fitted with a sum of up to six exponentials using the R luminescence package (Kreutzer et al., 2023), with the most appropriate fit selected using the goodness of fit (pseudo R^2 parameter).

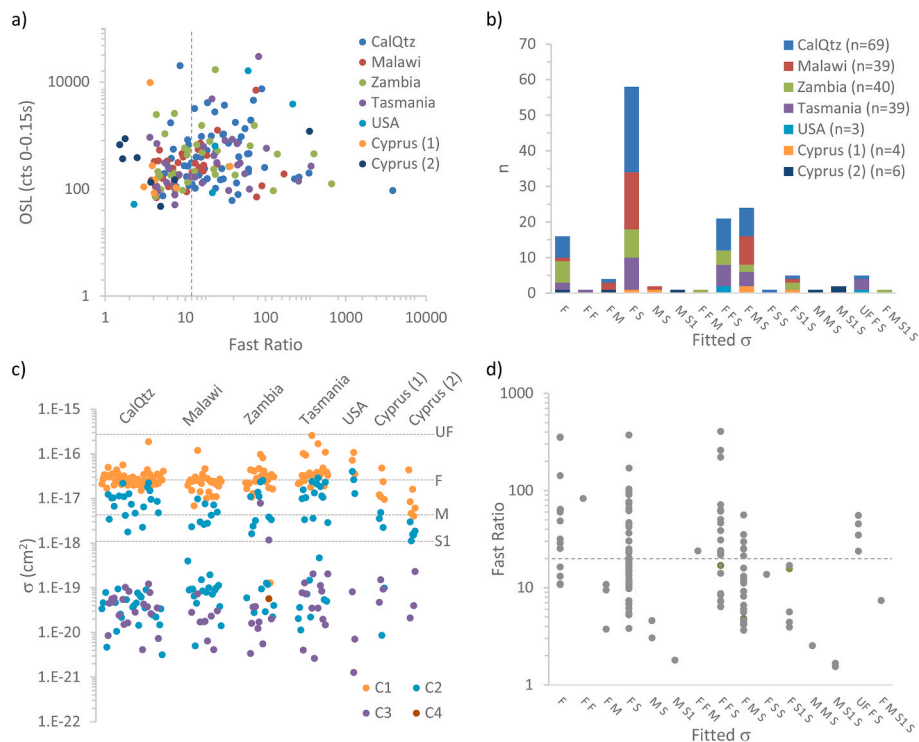


Fig. 2. a) OSL signal intensity (counts from the first channel of stimulation (0–0.15 s)) plotted as a function of fast ratio ($n = 214$). A reference line showing a fast ratio of 20 is shown. b) Histogram ($n = 142$) of the combination of components fitted through curve convolution for single grain OSL signals, where F = Fast (σ in the range of $(1.0\text{--}9.99) \times 10^{-17} \text{ cm}^2$), M = Medium ($\sigma = (2.70\text{--}9.99) \times 10^{-18} \text{ cm}^2$), S1 = Slow 1 ($\sigma = (1.00\text{--}2.69) \times 10^{-18} \text{ cm}^2$), S ($\sigma < 9.99 \times 10^{-19} \text{ cm}^2$) and UF = Ultrafast ($\sigma > 1.0 \times 10^{-16} \text{ cm}^2$), using the multi-grain σ values of Jain et al. (2008) and Durcan and Duller (2011). c) Photo ionisation cross-sections (σ) derived from curve deconvolution of 142 single grain quartz OSL signals. σ values are plotted according to size, from largest (C1) to smallest (C4), and multi-grain σ values for the F, M and S (Durcan and Duller, 2011) and the UF (Jain et al., 2008) are shown for reference. d) The fast ratio as a function of the number and combination of quartz OSL components fitted, with the fast ratio of 20 reference line shown. In b) and d), the number and combination of components fitted is indicated. For example, where 'F' means only a fast component was fitted, and 'F M S' indicated three components, a fast, medium, and slow, were fitted.

Only signals where the best R^2 fit exceeded 0.8 were included in analysis, and this excluded 72 signals, primarily with low sensitivity (typically with <100 counts in channel 1 of stimulation). In total, 142 signals were analysed, and the number and combination of components fitted is shown in Fig. 2b, as well as the calculated photo ionisation cross-sections (σ) in Fig. 2c. For the most part, single grain signals are fitted with either 2 (65/142) or 3 (60/142) components (Fig. 2b), with only 1 signal being best fit by the sum of 4 exponentials, and 16 signals fitted with a single exponential (always the fast component; Fig. 2b). Calculated σ values were used to define the components using published multi-grain values as a guide (Jain et al., 2003, 2008; Durcan and Duller, 2011), with σ values in the range of 10^{-17}cm^2 defining the fast component (σ_F), $(2.70\text{--}9.99) \times 10^{-18}\text{cm}^2$ the medium component (σ_M), $(1.00\text{--}2.69) \times 10^{-18}\text{cm}^2$ the slow1 component (σ_{S1}), and values of $<10^{-19}\text{cm}^2$ were broadly defined as a slow component (σ_S). For some signals, an ultra-fast component (σ_{UF}) with a σ in the range of 10^{-16}cm^2 was observed. A total of 15 combinations of number/composition of components were fitted, and the fast component was fitted for most signals (only 6 of the 142 OSL signals did not have a fast component fitted). For this dataset the modal fit is a 2 component fast and slow fit with 41% of signals from almost the full range of samples best fit this way (Fig. 2b). The second most common fit is a three component fast, medium, and slow fit, although this is only seen for 24 (17%) of signals. The fast, medium, and slow component fit is hypothesized to be typical of multi-grain quartz OSL signals (e.g. Bailey et al., 1997), however the fitting of this combination of components is not commonly observed for the single-grain OSL signals considered in this study.

In this dataset of 142 grains for which components were fitted, average σ values for the fast ($\sigma_F = (2.72 \pm 0.16) \times 10^{-17}\text{cm}^2$), medium ($\sigma_M = (6.77 \pm 0.99) \times 10^{-18}\text{cm}^2$), and slow1 ($\sigma_{S1} = (2.35 \pm 0.69) \times 10^{-18}\text{cm}^2$) components are calculated. These are in line with previously published values from multi-grain signals (Jain et al., 2003; Singarayer and Bailey, 2003; Durcan and Duller, 2011). In addition, 5 signals (4

from Tasmania, 1 from USA) yield σ values in the range of the ultrafast component (10^{-16}cm^2), with an average of σ_{UF} of $(1.53 \pm 0.27) \times 10^{-16}\text{cm}^2$. Investigation of the ultrafast component in OSL-based studies is not common, with signals from the ultrafast component not frequently observed and/or reported, but the σ_{UF} values reported in this study compare well with those of Jain et al. (2008) of $(2.68 \pm 0.03) \times 10^{-16}\text{cm}^2$ and $(2.76 \pm 0.02) \times 10^{-16}\text{cm}^2$ derived from multigrain signals of Swedish and Korean quartz samples. Although in their study, Jain et al. (2008) found that a pre-heat of at least 200°C was sufficient to de-trap signal from their ultrafast component, and given the 220°C pre-heat used in this study, the ultrafast component observed here may not be the same as those observed by Jain et al. (2008). The fitting of a σ_F is almost ubiquitous across the dataset, with all but 7 of the 142 signals being fitted with a component of the order of 10^{-17}cm^2 , these signals are from the Calibration Quartz and samples from Zambia, Tasmania, and Cyprus (2), and are evident in Fig. 2c. Despite the presence of a fitted fast component in nearly all grains in this dataset, as noted, almost 50% of signals fail the fast ratio (e.g. Fig. 2a). In Fig. 2d, the fast ratio is plotted as a function of the components fitted, and it is evident that fast ratios across the full range of 0 to >20 can be calculated for signals with a fast component, demonstrating the importance of the trapped charge populations associated with each OSL component, as well as the presence or absence of a particular component. There are small number of signals fitted with only a fast component which have fast ratios <20 (Fig. 2d). For these four signals, the fast ratios range between 10.7 and 16. Reassuringly, those signals without a fast component have fast ratios below 20. This suggests that the presence of a fast component does not necessarily equate to the dominance of signal from the fast component in the initial part of the signal.

Amongst others, Spooner (1994) hypothesize a relationship between the 325°C TL peak and the OSL signal. In Fig. 3, the percentage contributions from different TL peaks to the total TL glow curve is plotted for signals with differing component compositions. In Fig. 3d, the 325°C TL

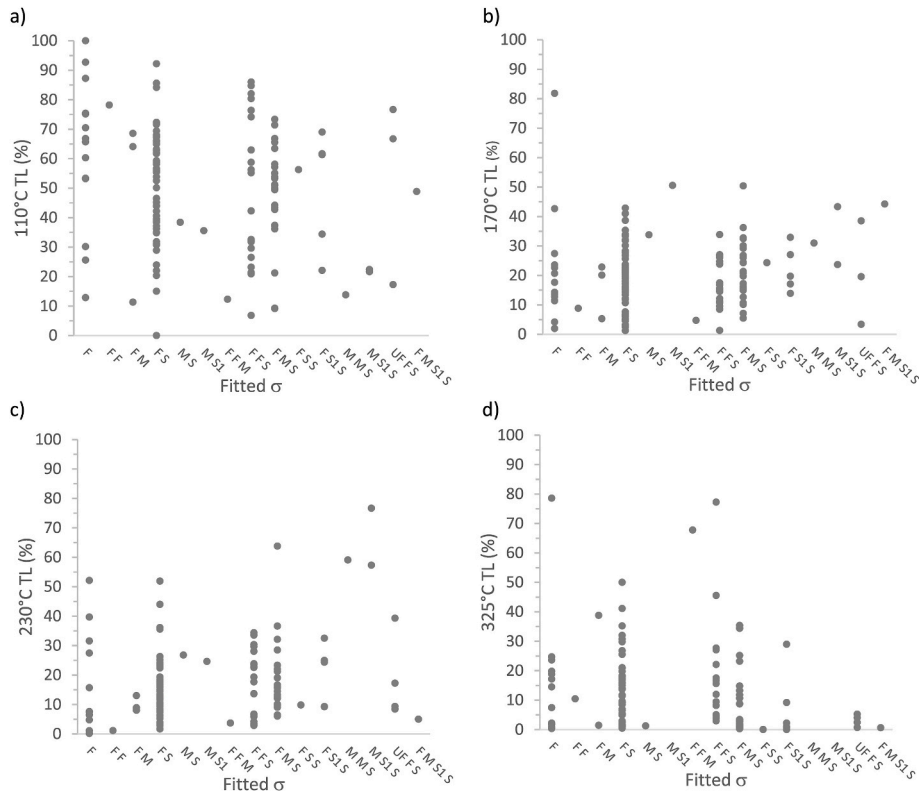


Fig. 3. The percentage contribution of background subtracted counts from the TL peaks a) 110°C , b) 170°C , c) 230°C , and d) 325°C to the total TL counts, plotted as a function of the number and combination of quartz OSL components fitted. For some signals, a discernible TL peak above background levels was not observed. Counts were integrated from the area $\pm 15^\circ\text{C}$ around the TL peak temperature.

contribution is shown to be highly variable, ranging between 0 and 80%. A contribution from this peak is notably very low or absent for the OSL signals without a fast component (Fig. 3d), and these signals tend to have a relatively high contribution from the 230 °C TL peak (Fig. 3c). Variability in the TL glow curve shape is the norm rather than exception, and Fig. 3 indicates variation in glow curve shape for the suite of signals measured, and an absence of a clear trend in TL contributions according to OSL component number and combination.

Amongst the dataset, there are 22 signals which have two fast components fitted. 21 of these signals are best fitted with 3 components (fast, fast, slow), with these signals drawn from a range of samples (Fig. 2b), and 1 signal from the Tasmanian sample is best fitted with a 2 component fast, fast combination (Fig. 2b). These double-fast signals are visible in Fig. 2a, where the two largest σ values (C1 and C2) plot above 10^{-17} cm^2 , and individual σ values are provided in Table S2. At present, the presence of two fast components is difficult to explain. There is a possibility that some of the larger fast components (in the range $7.0\text{--}9.9 \times 10^{-17} \text{ cm}^2$) are ultra-fast components, and similarly some of the smaller cross-section values may be indicative of the medium component. It is also possible that an unstable component is present, and pulse annealing data was used to explore the possible presence of an unstable fast component in these signals, which has been reported from Chinese sediments by Fan et al. (2011), where they calculate a $\sigma_{\text{F-unstable}}$ value of $(2.51 \pm 0.22) \times 10^{-17} \text{ cm}^2$. They use a ratio (R_T) of the L_x/T_x values from the 240 °C and 280 °C cycles in the pulse anneal test (where R_T is $\text{OSL}_{280^\circ\text{C}}/\text{OSL}_{240^\circ\text{C}}$), noting that although this pair of temperatures was chosen arbitrarily, for thermally stable OSL signals heating to 280 °C should not impact the OSL signal significantly. Therefore R_T ratios of 1 are taken to indicate stability, and less than 0.9 (including uncertainty) are indicative of the presence of an unstable signal. In Fig. 4, example pulse annealing curves for a selection of signals in this study are shown (Fig. 4a), along with the R_T ratios plotted as a function of number and presence of components (Fig. 4b). For this suite of signals, the majority of signals pass the R_T ratio (example pulse anneal curve are shown in

Fig. 4c), and there are 24 signals which have an R_T lower than 0.9 (Fig. 4d). For the 6 signals with no fast component fitted, 5 have R_T ratios which indicate thermal instability (e.g. <0.9). For the remaining 19 signals with R_T ratios <0.9 , these signals are drawn from a range of component combinations (Fig. 4b). There is no systematic trend for signals with a double-fast component to fail the ratio, although some fast, fast, slow component signals do (Fig. 3b), and this is similar for the signals with an ultrafast component fitted (Fig. 4b). For the majority of samples, signal intensity was not sufficient for the mathematical fitting of the pulse annealing data to derive kinetic values such as trap depth and frequency factor which would confirm signal lifetime and therefore stability. However, the R_T ratios calculated here are interpreted as an indication of general signal stability for the analysed signals, and the presence of an unstable fast component cannot be concluded.

The presence of an unstable, ultrafast component in the quartz OSL signal has occasionally been reported (e.g. Jain et al., 2008; Ferreira de Souza et al., 2014), and as discussed, we note 6 signals in this study which have σ_{UF} values fitted. These signals do not notably stand out in the dataset: fast ratios are in the range of 20–50 (Fig. 2d), signal sensitivity is not overly high (on average 270 ± 184 counts in the first channel of stimulation (0–0.15s)), and characteristic doses (D_0) are in the range of ~50–175 Gy (see section 3.3). Ferreira de Souza et al. (2014) find that the ultrafast component and the 300 °C TL peak have similar thermal stabilities, and suggest a relationship between the two. Analysis of the corresponding TL glow curves shows that for these signals, there is a negligible contribution from the 300 °C TL peak to the total TL, with less than 6% of the total TL signal originating from this peak (285–315 °C). Similarly, the 325 °C contributes relatively little to the total TL for these signals (Fig. 3d), with greater contributions seen from the 110 °C, 170 °C and 230 °C (Fig. 3a–c). This better corresponds with Jain et al.’s (2008) suggestion that the ultrafast component corresponds to shallower traps, i.e. lower temperature TL peaks. We note that the sensitivity of the single grain signals is not high and there are only 6 signals which have a fitted ultrafast component.

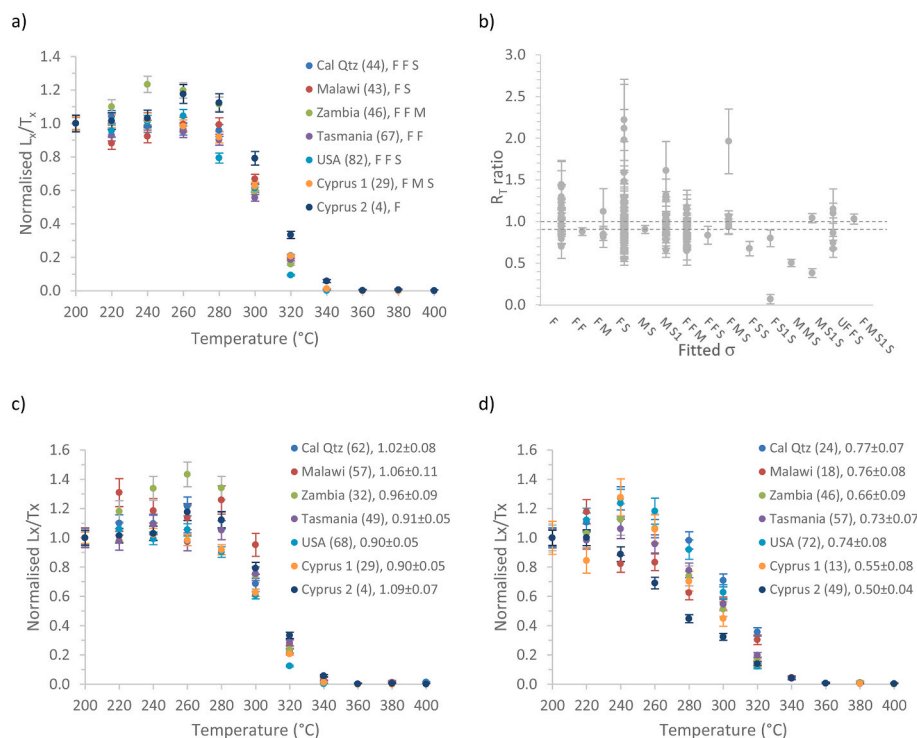


Fig. 4. a) Example pulse anneal curves for the brightest signal from each sample. The sample grain number and combination of fitted components are shown in the legend. b) The R_T ratio of [Fan et al. \(2011\)](#) from 142 signals, plotted as a function of the number and combination of quartz OSL components fitted. In c) and d) examples of signals with pulse anneal curves which pass the R_T (within 10% of unity including uncertainties) and fail the R_T (<0.9) are shown. The grain number and R_T are shown in the legend.

A medium component is observed for 38 of 142 signals in this dataset, and this average σ_{MIS} (6.66 ± 0.99) $\times 10^{-18} \text{ cm}^{-2}$. This component is fitted across the suite of samples used in this study, apart from the USA sample (Fig. 2c), although only 3 signals from this sample were of sufficient sensitivity for OSL curve deconvolution. Considering the TL glow curves, the defect associated with the 170 °C TL peak has recently been hypothesized as important for the production of the medium component OSL signal, whereby this signal is produced as a result of the phototransfer of fast component signal through the 170 °C trap (Wang et al., 2015; Peng and Wang, 2020). However, there is no detectable relationship between 170 °C TL contribution to the total TL signal and the presence or absence of a fitted medium component in the OSL signal (Fig. 2b). Like the conclusion of Durcan and Duller (2022) where analysis was limited to the 50 brightest OSL grains, with this more populated dataset, there remains a lack of a clear relationship between the relative contribution of the 170 °C TL peak to the total TL glow curve, which suggests that for this suite of samples, it is likely there are other mechanisms of medium component OSL signal production.

A slow1 component was fitted in 9 signals and at least 1 slower component (of the orders 10^{-19} cm^{-2} to 10^{-21} cm^{-2}) was calculated for all but 20 of the 142 signals where signals were mathematically deconvolved. This suggests that charge storage in deeper traps within the quartz crystal is a common phenomenon, although the traps responsible for these slow components are variable. Calculated σ_{S} values are plotted in Fig. 2c, although should be considered indicative, because the OSL stimulation time (100 s of stimulation using 30 mW/cm² power LEDs) used in this study is not sufficient to fully deplete the charge in the slower components (particularly the slow3 and 4; see Durcan and Duller, 2011), and therefore σ_{S} values may not be precise.

3.3. Characteristic dose

The upper limit of luminescence dating is constrained by the saturation limit of the OSL signal, whereby charge no longer accumulates in the traps of interest despite ongoing irradiation. Where luminescence dose response curves are described mathematically with a saturating exponential function, the asymptote represents the maximum luminescence intensity produced in response to dose and is termed I_{max} (e.g. Wintle and Murray, 2006). For defining signal saturation, Wintle and Murray (2006) suggest the use of the characteristic dose (D_0) as a reference point, where twice the characteristic dose ($2D_0$) corresponds to the dose at which the signal intensity reaches $\sim 85\%$ of I_{max} . For the dating of samples, signals where the natural signal exceeds the $2D_0$ threshold of the dose response curve, or where a natural signal cannot be interpolated, are often considered to be in saturation (e.g. Wintle and Murray, 2006). This is the subject of debate however, with some studies published ages using D_e values that exceed $2D_0$. The use of $2D_0$ as a rejection criterion in dating is not automatically used in the luminescence dating community, although it has been noted that the inclusion of saturated signals in D_e distributions can lead to biases in D_e (e.g. Murray and Funder, 2003; Thomsen et al., 2016; Murray et al., 2021). D_0 values from multi-grain, fast component-dominated OSL signals have been reported to be in the region of 50–100 Gy (e.g. Preusser et al., 2009; Wintle and Adamiec, 2017), although a greater range of D_0 values have been reported from single grain studies (e.g. Duller, 2012; Chapot et al., 2022; Hu et al., 2021).

In this study D_0 values were derived from the fitting of dose response curves with a single saturating exponential function, with dose response curves built using doses of up to 1000 Gy to ensure OSL signal saturation. Calculated D_0 values range between 9 ± 9 Gy (Calibration Quartz) and 442 ± 24 Gy (Cyprus 1) with an average of 107 ± 80 Gy ($n = 212$). Additionally, two extremely high D_0 values of 629 ± 871 Gy and 927 ± 2605 Gy were calculated, although are not included in discussion given the high associated uncertainties, which is due to low signal sensitivity and a poor fit on the dose response curve. The calculated average is comparable with multi-grain D_0 ranges frequently published for fast

component-dominated OSL signals (e.g. the 50–100 Gy range cited in Wintle and Murray, 2006). At a single grain scale, greater variability in dose response curve form has been reported (e.g. Yoshida et al., 2000) and single grain D_0 value ranges of c. 30–200 Gy have been calculated by Hu et al. (2021) and c. 10 - >100 Gy (average 47 Gy) by Duller (2012). As shown in Fig. 5a, in this study the distribution of D_0 values is left-skewed, reflected by a median D_0 value of 84 Gy and an interquartile range of 52–140 Gy. High D_0 values are relatively rare, with only 22 grains (c. 10%) having D_0 values exceeding 200 Gy, 10 grains (c. 5%) >300 Gy, and only 1 grain exceeding 400 Gy. Considering intra-sample variability, it is evident from the data in Fig. 5a, that D_0 values vary across a broad range for all seven samples measured. For samples with a higher number of signals measured D_0 average and standard deviation vary: Calibration Quartz ($n = 69$) is 71 ± 58 Gy, Malawi ($n = 39$) is 158 ± 77 Gy, Zambia ($n = 41$) is 90 ± 68 Gy, and Tasmania ($n = 39$) is 131 ± 145 Gy. For samples with a lower yield of signals, USA ($n = 10$) is 100 ± 70 Gy, and Cyprus 1 ($n = 7$) and Cyprus 2 ($n = 8$) are 257 ± 140 Gy and 174 ± 179 Gy respectively. Example individual dose response curves for selected individual grains of the Zambian sample are shown in Fig. 5b.

In Fig. 5, the relationship between D_0 and signal intensity, the fast ratio, and the number and presence of quartz OSL components (Fig. 5e) is explored. There is no obvious relationship between D_0 and OSL signal intensity (Fig. 5c), neither is there an obvious relationship between fast ratio and D_0 for the overall dataset (Fig. 5d). Interestingly, signals which have a high D_0 are much less likely to have a fast ratio >20, indicative of dominance of the fast component. As discussed, for the 214 signals providing a luminescence signal in response to dose, 50.5% have a calculated fast ratio >20. However, for the 35 signals where D_0 exceeds 150 Gy, only 9 (26%) are dominated by the fast component, and where D_0 is greater than 200 Gy (15 signals), only three signals (20%) are fast dominated. The higher saturation of the slower OSL components when compared to the fast component has been observed previously in multi-grain signals (e.g. Bailey et al., 1997; Rhodes et al., 2006). In contrast, for the 40 signals with D_0 in the range of 100–150 Gy, 22 have fast ratios indicative of dominance of the fast component. These high dose D_0 signals are not characterised by a lack of a fitted fast component (Fig. 5e), and for the 15 signals where $D_0 > 200$ Gy, only 2 signals lack a fitted fast, and are instead fitted with a medium and slow 1 component only (Fig. 5e). These high dose D_0 signals are drawn from a range of samples (Fig. 5d) and therefore, this does not appear to be a sample-specific feature. Whilst only a small proportion of the signals analysed yield D_0 values greater than 150 Gy, the data presented here indicate that for the most part, high D_0 signals are not dominated by the fast component. It may therefore be the case that there is an upper limit to D_0 of fast dominated OSL signals of ~ 150 Gy.

4. Conclusions

In this study, EMCCD imaging of heated single grain OSL signals has been used to investigate the variability of signal intensities, the fast ratio, the number and presence of quartz OSL components including the calculation of photo ionisation cross-sections, and characteristic doses. TL signal intensities have also been considered. Whilst some of these parameters have been considered at single grain scales previously, the imaging of signals rather than the use of the Risø focussed laser system for measurement allows a view of intrinsic variability of signals without the increased uncertainties associated with optical flux of the laser.

Using the same dataset of single grain signals from 7 samples, including calibration quartz, this study has extended the analysis of Durcan and Duller (2022). Intra-sample variability in the intensity of TL and OSL signals is observed, with recorded counts varying of the order 10^3 – 10^4 counts (for the TL glow curve and the first channel of stimulation of the OSL signal). Comparison of the two shows no clear relationship however between TL and OSL. For some signals, TL signals are observed with no detectable OSL and vice versa. That a sample should

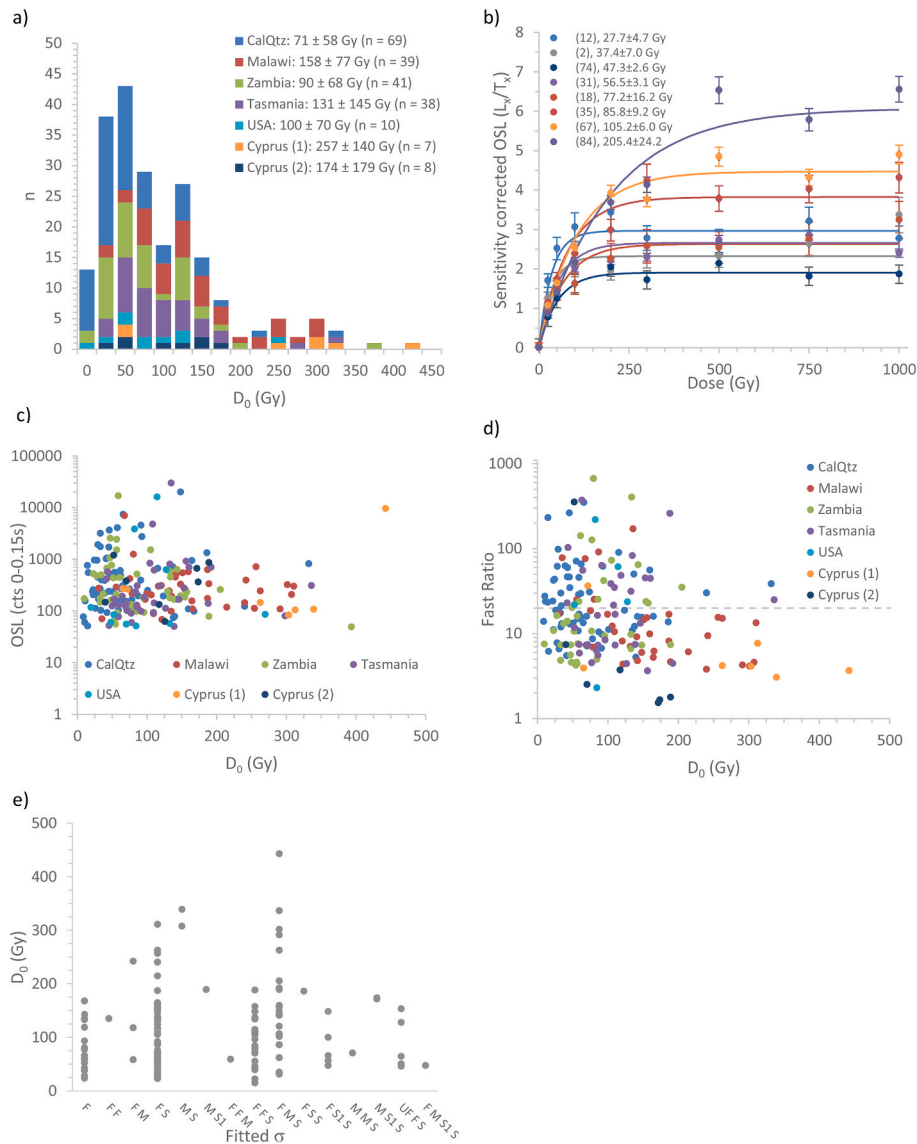


Fig. 5. a) Histogram of the D_0 values calculated by sample for the dataset ($n = 212$). The sample average D_0 and standard deviation are shown in the legend. b) Dose response curves for selected single grains of the Zambian sample (grain number shown in parentheses in the legend), where D_0 values between 10 and 393 Gy were calculated (average 90 ± 68 Gy). Dose response curves were fitted with a single saturating exponential. The relationship between D_0 and signal intensity and the fast ratio are shown in c) and d), with a reference line for a fast ratio of 20 shown in d). In e), the D_0 values are plotted by number and combination of quartz OSL components fitted using curve deconvolution.

emit UV OSL and not UV TL is feasible, given the broad emission spectra of quartz TL, although the reason why UV TL is emitted not UV OSL for the same grain is less clear given the reported UV only emission of quartz OSL. This reflects the complexity of de-trapping and recombination processes, where recombination does not always give rise to the production of luminescence.

The curve deconvolution of signals ($n = 142$ grains) shows that at single grain scales of analysis, it is most common for either two or three quartz OSL components to be fitted. The single grain photo ionisation cross-section values calculated compare well with published values from multi-grain signals. The most common fit is a 2 component fit of a fast and slow component (41% of signals), and the fitting of the 'classic' 3 component fast, medium, and slow component often evident for multi-grain signals is not commonly observed in this dataset. The fast component is a feature of nearly all signals in this dataset, although the presence of the medium is more variable. We report the presence of signals containing two fast components, although there is not evidence from the R_T ratio that these double-fast signals contain an unstable fast

component (e.g. Fan et al., 2011). Although rare in this dataset, the ultrafast component is also observed for a small number of signals in this study. Interestingly, the presence of a fitted fast component does not necessarily correspond with that signal passing the fast ratio, and given that there is no relationship between the fast ratio and signal intensity, this highlights the importance of the fast ratio as a tool for assessing the dominance of signal from the fast component in the initial part of the OSL signal when using a late background for signal integration.

Characteristic doses are calculated from dose response curves with a maximum dose of 1000 Gy. Intra-sample variability in D_0 is again a feature of the samples considered in this study. Individual D_0 values range between 9 and 442 Gy, with an average of 107 ± 80 Gy. Comparison of D_0 and the fast ratio suggests that for signals where D_0 values are greater than ~ 150 Gy, the fast ratio is likely to be under 20, suggesting that signal from the fast component is not dominant in the initial part of the signal. Therefore, from this dataset, there is the suggestion that ~ 150 Gy is the upper limit for fast component-dominated signals, and places the upper dateable limit ($2D_0$) at 300 Gy, when using the fast

component.

In conclusion, a range of heated quartz luminescence signal properties have been considered at a single grain scale using EMCCD imaging. Variability is the norm rather than the exception across the suite of properties and samples considered, and this work demonstrates that the luminescence characteristics of quartz are variable and diverse.

CRedit authorship contribution statement

Julie A. Durcan: Conceptualization, Data curation, Formal analysis, Funding acquisition, Investigation, Methodology, Writing – original draft, Writing – review & editing. **Geoff A.T. Duller:** Conceptualization, Formal analysis, Funding acquisition, Resources, Software, Supervision, Writing – original draft.

Declaration of competing interest

The authors declare that they have no known competing financial interests or personal relationships that could have appeared to influence the work reported in this paper.

Data availability

Data will be made available on request.

Acknowledgements

We thank Helen Roberts and Richard Bailey for the use of their quartz samples. We also thank the reviewers and editors for their time, as well as their comments and suggestions which have greatly improved this manuscript. JAD acknowledges the support of the Quaternary Research Association to attend the 17th International Luminescence and Electron Spin Resonance Dating conference in Copenhagen, Denmark, and Leverhulme Trust grant RPG-2019-392. Sebastian Kreutzer is thanked for his advice regarding the R Luminescence package. Research in Next Generation Luminescence methods in Aberystwyth is supported by NERC grant CC003 to GATD, by HEFCW infrastructure funding for SPARCL (SPATIally Resolved geochronoLOGY), and by an AHRC grant (AH/N008804/1).

Appendix A. Supplementary data

Supplementary data to this article can be found online at <https://doi.org/10.1016/j.radmeas.2024.107260>.

References

- Adamiec, G., 2000. Variations in luminescence properties of single quartz grains and their consequences for equivalent dose estimation. *Radiat. Meas.* 32, 427–432.
- Adamiec, G., 2005. OSL decay curves-relationship between single- and multiple-grain aliquots. *Radiat. Meas.* 39, 63–75.
- Bailey, R.M., 2001. Towards a general kinetic model for optically and thermally stimulated luminescence of quartz. *Radiat. Meas.* 33, 17–45.
- Bailey, R.M., 2010. Direct measurement of the fast component of quartz optically stimulated luminescence and implications for the accuracy of optical dating. *Quat. Geochronol.* 5, 559–568.
- Bailey, R.M., Smith, B.W., Rhodes, E.J., 1997. Partial bleaching and the decay form characteristics of quartz OSL. *Radiat. Meas.* 27, 123–126.
- Bøtter-Jensen, L., Duller, G.A.T., Murray, A.S., 2000. Advances in luminescence measurement systems. *Radiat. Meas.* 32, 523–528.
- Bøtter-Jensen, L., Thomsen, K.J., Jain, M., 2003. Review of optically stimulated luminescence (OSL) instrumental developments for retrospective dosimetry. *Radiat. Meas.* 45, 253–257.
- Bulur, E., Duller, G.A.T., Solongo, S., Bøtter-Jensen, L., Murray, A.S., 2002. LM-OSL from single grains of quartz: a preliminary study. *Radiat. Meas.* 35, 79–85.
- Chapot, M.S., Duller, G.A.T., Barham, L.S., 2022. Challenges of dating quartz OSL samples with saturated grains: Lessons from single-grain analyses of low dose-rate samples from Victoria Falls, Zambia. *Quat. Geochronol.* 72, 101344.
- Choi, J.H., Murray, A.S., Cheong, C.S., Hong, D.G., Chang, H.W., 2003. The resolution of stratigraphic inconsistency in the luminescence ages of marine terrace sediments from Korea. *Quat. Sci. Rev.* 22, 1201–1206.
- Duller, G.A.T., 2008. Single-grain optical dating of Quaternary sediments: why aliquot size matters in luminescence dating. *Boreas* 37, 589–612.
- Duller, G.A.T., 2012. Improving the accuracy and precision of equivalent doses determined using the optically stimulated luminescence signal from single grains of quartz. *Radiat. Meas.* 47, 770–777.
- Duller, G.A.T., Bøtter-Jensen, L., Murray, A.S., Truscott, A.J., 1999. Single grain laser luminescence (SGLL) measurements using a novel automated reader. *Nucl. Instrum. Methods B* 33, 506–514.
- Duller, G.A.T., Bøtter-Jensen, L., Murray, A.S., 2003. Combining infrared- and green-laser stimulation sources in single-grain luminescence measurements of feldspar and quartz. *Radiat. Meas.* 37, 535–541.
- Durcan, J.A., Duller, G.A.T., 2011. The fast ratio: a rapid measure for testing the dominance of the fast component in the initial OSL signal from quartz. *Radiat. Meas.* 46, 1065–1072.
- Durcan, J.A., Duller, G.A.T., 2022. The variability of single grain quartz luminescence properties investigated using EMCCD imaging. *Radiat. Meas.* 153, 10678.
- Fan, A., Li, S.-H., Li, B., 2011. Observation of unstable fast component in OSL of quartz. *Radiat. Meas.* 46, 21–28.
- Ferreira de Souza, L.B., Guzzo, P.L., Khoury, H.J., 2014. OSL and photo-transferred TL of quartz single crystals sensitized by high-dose of gamma-radiation and moderate heat-treatments. *Appl. Radiat. Isot.* 94, 93–100.
- Gray, H.J., Jain, M., Sawakuchi, A.O., Mahan, S.A., Tucker, G.E., 2019. Luminescence as a sediment tracer and provenance tool. *Rev. Geophys.* 57, 987–1017.
- Hashimoto, T., Hayashi, Y., Koyanagi, A., Yokosaka, K., Kimura, K., 1986. Red and blue colouration of thermoluminescence from natural quartz sands. *Nucl. Tracks Radiat. Meas.* 11, 229–235.
- Hu, Y., Li, B., Jacobs, Z., 2021. Single-grain quartz OSL characteristics: testing for correlations within and between sites in asia, europe and africa. *Methods. Protoc.* 3, 2.
- Huntley, D., Godfrey-Smith, D., Haskell, E., 1991. Light-induced emission spectra from some quartz and feldspars. *Int. J. Radiat. Appl. Instrum. Nucl. Tracks Radiat. Meas.* 18, 127–131.
- Jain, M., Murray, A.S., Bøtter-Jensen, L., 2003. Characterisation of blue-light stimulated luminescence components in different quartz samples: implications for dose measurement. *Radiat. Meas.* 37, 441–449.
- Jain, M., Murray, A.S., Bøtter-Jensen, L., Wintle, A.G., 2005. A single aliquot regenerative-dose method based on IR (1.49 eV) bleaching of the fast OSL component in quartz. *Radiat. Meas.* 39, 309–318.
- Istratov, A.A., Vyvenko, O.F., 1998. Exponential analysis in physical phenomena. *Rev. Sci. Instrum.* 70, 1233–1257.
- Jacobs, Z., Duller, G.A.T., Wintle, A.G., Henshilwood, C.S., 2006. Extending the chronology of deposits at Blombos Cave, South Africa, back to 140 ka using optical dating of single and multiple grains of quartz. *J. Hum. Evol.* 51, 255–273.
- Jain, M., Choi, J.H., Thomas, P.J., 2008. The ultrafast OSL component in quartz: origins and implications. *Radiat. Meas.* 43, 709–714.
- Kitis, G., Kiyak, N., Polymeris, G.S., Tsirliganis, N.C., 2010. The correlation of fast OSL component with the TL peak at 325°C in quartz of various origins. *J. Lumin.* 130, 298–303.
- Kook, M., Lapp, T., Murray, A.S., Thomsen, K.J., Jain, M., 2015. A luminescence imaging system for the routine measurement of single-grain OSL dose distributions. *Radiat. Meas.* 81, 171–177.
- Kook, M., Lapp, T., Murray, A.S., Thomsen, K.J., Jain, M., 2018. A luminescence imaging system for the routine measurement of single-grain OSL dose distribution. *Radiat. Meas.* 81, 171–177.
- Krbetschek, M.R., Gotze, J., Dietrich, A., Trautmann, T., 1997. Spectral information from minerals relevant for luminescence dating. *Radiat. Meas.* 27, 695–748.
- Kreutzer, S., Burrow, C., Dietze, M., Fuchs, M., Schmidt, C., Fischer, M., Friedrich, J., Mercier, N., Philippe, A., Riedesel, S., Autzen, M., Mittelstrass, D., Gray, H., Galharret, J., 2023. Luminescence: comprehensive luminescence dating data analysis. R package version 0.9.22. <https://CRAN.R-project.org/package=Luminescence>.
- Kristensen, J.A., Thomsen, K.J., Murray, A.S., Buylaert, J.-P., Jain, M., Breuning-Madsen, H., 2015. Quantification of termite bioturbation in a savannah ecosystem: application of OSL dating. *Quat. Geochronol.* 30, 334–341.
- Lomax, J., Mittelstraß, Kreutzer, S., Fuchs, M., 2015. OSL, TL and IRSL emission spectra of sedimentary quartz and feldspar samples. *Radiat. Meas.* 81, 251–256.
- Martini, M., Fasoli, M., Galli, A., 2009. Quartz OSL emission spectra and the role of [AlO₄]⁻ recombination centres. *Radiat. Meas.* 44, 458–461.
- McKever, S.W.S., Morris, M.F., 1994. Computer simulations of optical bleaching of TL and OSL signals. *Radiat. Meas.* 23, 301–306.
- Murray, A.S., Wintle, A.G., 2000. Luminescence dating of quartz using an improved single-aliquot regenerative-dose protocol. *Radiat. Meas.* 32, 57–73.
- Murray, A.S., Arnold, L.J., Buylaert, J.P., Guerin, G., Qin, J., Singhvi, A.K., Smedley, R. K., Thomsen, K.J., 2021. Optically stimulated luminescence dating using quartz. *Nat Rev Methods Primers* 1, 72.
- Murray, A.S., Funder, S., 2003. OSL dating of a Danish Eemian coastal marine deposit: a test of accuracy. *Quat. Sci. Rev.* 22, 1177–1183.
- Peng, J., Li, B., 2017. Single-aliquot regenerative-dose (SAR) and standardised growth curve (SGC) equivalent dose determination in a batch model using the R Package 'numOSL'. *Ancient TL* 35, 32–53.
- Peng, J., Wang, X., 2020. On the production of the medium component in quartz OSL: experiments and simulations. *Radiat. Meas.* 138, 106448.
- Preusser, F., Chitamba, M.L., Gotte, T., Martin, M., Ramseyer, K., Sendezera, E.J., Susino, G.J., Wintle, A.G., 2009. Quartz as a natural luminescence dosimeter. *Earth Science Review* 97, 196–226.

- Rhodes, E.J., Singarayer, J.S., Raynal, J.P., Westaway, K.E., Sbihi-Alaoui, F.Z., 2006. New age estimates for the Palaeolithic assemblages and Pleistocene succession of Casablanca, Morocco. *Quat. Sci. Rev.* 25, 2569–2585.
- Rink, W.J., Rendell, H., Marseglia, E.A., Luff, B.J., Townsend, P.D., 1993. Thermoluminescence spectra of igneous quartz and hydrothermal vein quartz. *Phys. Chem. Miner.* 20, 353–361.
- Rodnight, H., Duller, G.A.T., Wintle, A.G., Tooth, S., 2006. Assessing the reproducibility and accuracy of optical dating of fluvial deposits. *Quat. Geochronol.* 1, 109–120.
- Rui, X., Li, B., Guo, Y.J., Zhang, J.F., Yuan, B.Y., Xie, F., 2019. Variability in the thermal stability of OSL signal of single-grain quartz from the Nihewan Basin, North China. *Quat. Geochronol.* 49, 25–30.
- Singarayer, J.S., Bailey, R.M., 2003. Further investigations of the quartz optically stimulated luminescence components using linear modulation. *Radiat. Meas.* 37, 451–458.
- Smedley, R.K., Buylaert, J.-P., Ujvari, G., 2019. Comparing the accuracy and precision of luminescence ages for partially-bleached sediments using single grains of K-feldspar and quartz. *Quat. Geochronol.* 53, 101007.
- Spooner, N.A., 1994. On the optical dating signal from quartz. *Radiat. Meas.* 23, 593–600.
- Thomsen, K.J., Murray, A.S., Jain, M., 2012. The dose dependency of the over-dispersion of quartz OSL single grain dose distributions. *Radiat. Meas.* 47, 732–739.
- Thomsen, K.J., Kook, M., Murray, A.S., Jain, M., Lapp, T., 2015. Single-grain results from an EMCCD-based imaging system. *Radiat. Meas.* 81, 185–191.
- Thomsen, K.J., Murray, A.S., Buylaert, J.P., Jain, M., Hansen, J.H., Aubry, T., 2016. Testing single-grain quartz OSL methods using sediment samples with independent age control from the Bordes-Fitte rockshelter (Roches d'Abilly site, Central France). *Quat. Geochronol.* 31, 77–96.
- Wang, X.L., Du, J.H., Adamiec, G., Wintle, A.G., 2015. The origin of the medium OSL component in West Australian quartz. *J. Lumin.* 159, 147–157.
- Wintle, A.G., Murray, A.S., 2006. A review of quartz optically stimulated luminescence characteristics and their relevance in single-aliquot regeneration dating protocols. *Radiat. Meas.* 41, 369–391.
- Wintle, A.G., Adamiec, G., 2017. Optically stimulated luminescence signals from quartz: a review. *Radiat. Meas.* 98, 10–33.
- Yoshida, H., Roberts, R.G., Olley, J.M., Laslett, G.M., Galbraith, R.F., 2000. Extending the age range of optical dating using single 'supergrains' of quartz. *Radiat. Meas.* 32, 439–446.